PERGAMON

Journal of Structural Geology 24 (2002) 937–952

JOURNAL OF STRUCTURAL GEOLOGY

www.elsevier.nl/locate/jstrugeo

Evolution and kinematics of an ancient décollement zone, mélange in the Shimanto accretionary complex of Okinawa Island, Ryukyu Arc

Kohtaro Ujiie*

Institute for Frontier Research on Earth Evolution, Japan Marine Science and Technology Center, 2-15 Natsushima-cho, Yokosuka 237-0061, Japan

Received 20 May 2000; revised 4 February 2001; accepted 8 July 2001

Abstract

Detailed structural analysis of the mélange in the Shimanto accretionary complex of Okinawa Island in the Ryukyu Arc elucidates the spatial distribution and temporal progression of décollement-related deformation. Early deformation took place in the footwall of the décollement and is characterized by subhorizontal layer-parallel extension and subsequent heterogeneous shear of partially lithified sediments, resulting in alternation of asymmetric (e.g. *S–C* fabrics) and layer-parallel extensional (boudined layers) fabrics. Mud intrusions suggest that high fluid pressure was locally generated in the footwall of the décollement. Late deformation is marked by the partitioning of deformation in the mélange: the lower structural level of the mélange was pervasively sheared along microfaults whereas the upper structural level was flattened with development of planar pressure solution cleavage. Because shear is concentrated in the lower structural level, late deformation is considered to have occurred in the hanging wall of the décollement. Kinematic indicators suggest that shear directions during décollement-related deformation reflect the relative plate motion during early Tertiary. After the mélange was incorporated into the accretionary prism, crenulation cleavage and cylindrical upright folds were formed under subhorizontal shortening.

Keywords: Accretionary complex; Décollement; Mélange

1. Introduction

At subduction zones, sediments on the oceanic plate may be offscraped at the toe of the accretionary prism or underthrust with the oceanic crust. Concerning the offscraped sediments, detailed deformation processes and associated changes in mechanical properties have been revealed both in modern (e.g. Karig, 1986; Maltman et al., 1993) and ancient (e.g. DiTullio and Byrne, 1990; Ujiie, K., 1997) accretionary prisms. The offscraped sediments are progressively lithified during accretion and deformed by subhorizontal shortening and subsequent development of imbricate structure (Ujiie, K., 1997).

Underthrust sediments are decoupled from the above offscraped sediments by a décollement that constitutes the plate boundary. At shallow structural levels, décollements are weak, composed of low density and underconsolidated materials (e.g. Moore et al., 1998; Moore, 2000), and may be conduits for fluid flow (e.g. Moore, 1989; Moore and Vrolijk, 1992). During deformation, décollement zones are inferred to progressively structurally thicken due to strain hardening associated with consolidation (Moore and Byrne, 1987; Kimura and Mukai, 1991). Thus, an ancient décollement zone is expected to record changes in mechanical properties, fluid behavior, and possibly the kinematics of the subducting plate during its progressive deformation. However, these changes in properties have not been fully documented. In particular, Ocean Drilling Program cores only penetrate shallow structural levels of modern accretionary prisms and allow one-dimensional sampling at relatively small scales. In contrast, mélanges developed in ancient accretionary prisms may provide an opportunity to record the spatial distribution and temporal progression of deformation associated with the décollement from shallow to deep structural levels. Moreover, they can be observed over a wider range of scales.

The Shimanto Belt is one of the typical ancient accretionary complexes in the world and is distributed along the Pacific side of southwest Japan and the northern and central Ryukyu Arc (Taira et al., 1988) (Fig. 1a). In the Shimanto Belt of Okinawa Island, a moderately metamorphosed sandstone–shale mélange is nearly continuously exposed at the southwestern end of the Shimanto Belt (Figs. 1b and 2). In this contribution, the evolution and kinematics of décollement-related deformation are described, based on

* Tel.: +81-468-67-9780; fax: +81-468-67-3409.
E-mail address: ujiiek@jamstec.go.jp (K. Ujiie).

0191-8141/02/$ - see front matter
PII: S0191-8141(01)00103-1

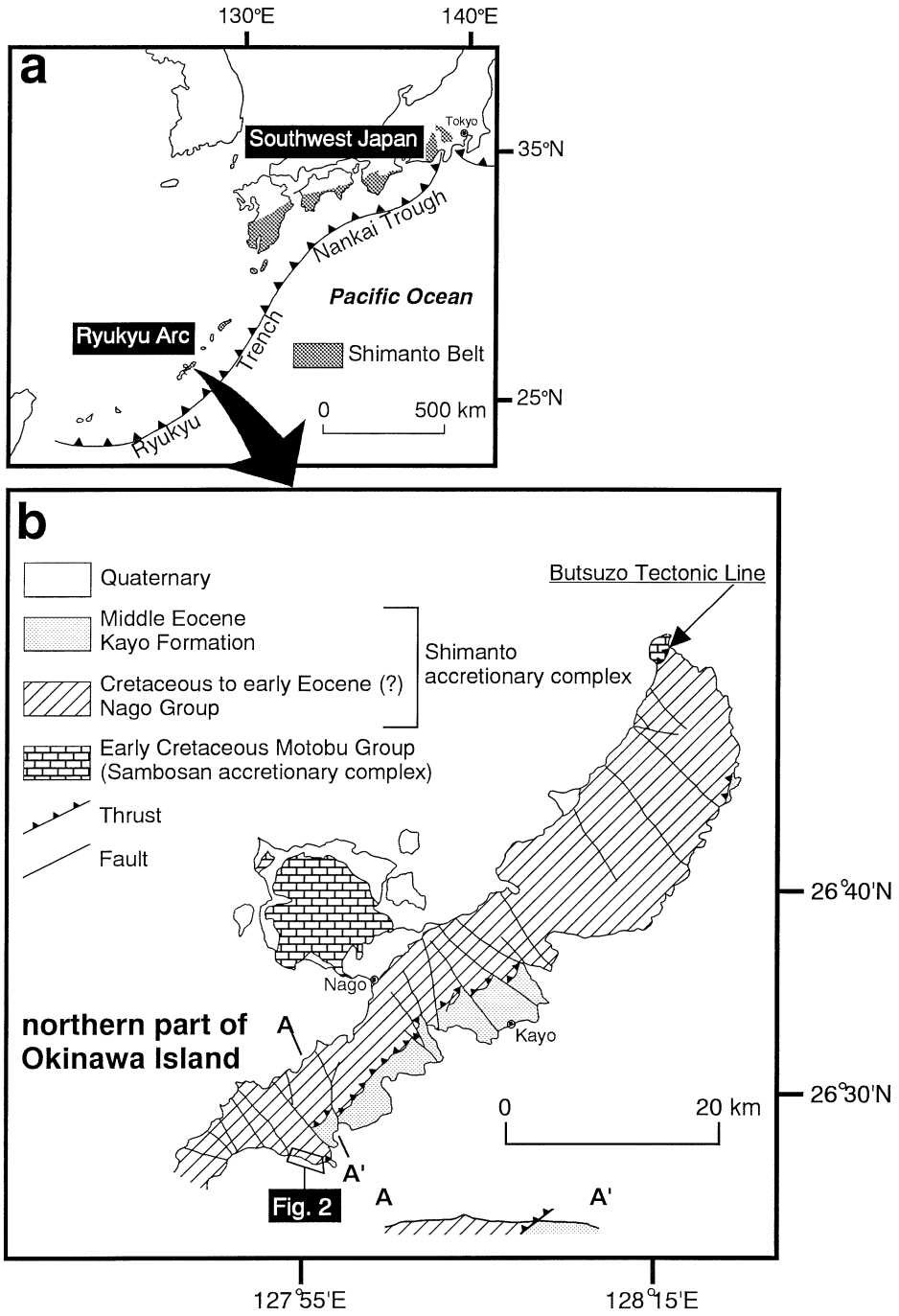

Fig. 1. (a) Distribution of the Shimanto Belt in southwest Japan and the Ryukyu Arc. (b) Tectonic map of the northern part of Okinawa Island compiled from Hashimoto and Nakagawa (1978) and Ujiie and Nishimura (1992).

structural analysis of mélange in the ancient accretionary prism of Okinawa Island.

2. Geological setting

The pre-Neogene basement rocks in Okinawa Island consist of the Sambosan and Shimanto accretionary complexes. These accretionary complexes are separated from each other by the NW-dipping thrust fault, called the Butsuzo Tectonic Line (Ujiie and Nishimura, 1992) (Fig. 1b).

The strata in the Shimanto accretionary complex are divided into the Cretaceous to early Eocene (?) Nago Group and the middle Eocene Kayo Formation. The Nago Group overlies the Kayo Formation along a NW-dipping thrust fault (Hashimoto and Nakagawa, 1978; Ujiie and Nishimura, 1992) (Fig. 1b), and is composed predominantly

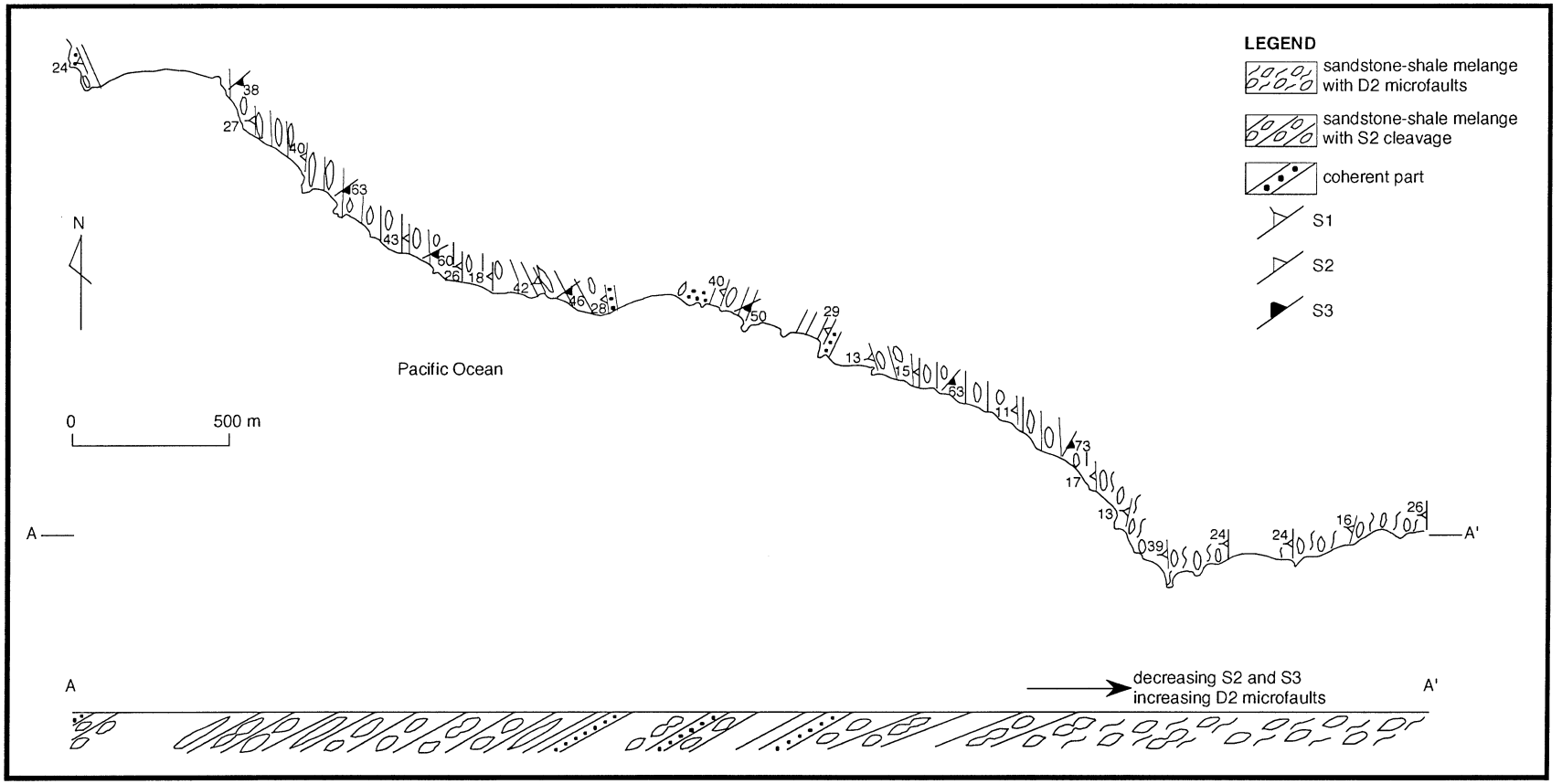

Fig. 2. Summarized geologic map and cross-section across the mélange. The location of the map is shown in Fig. 1.

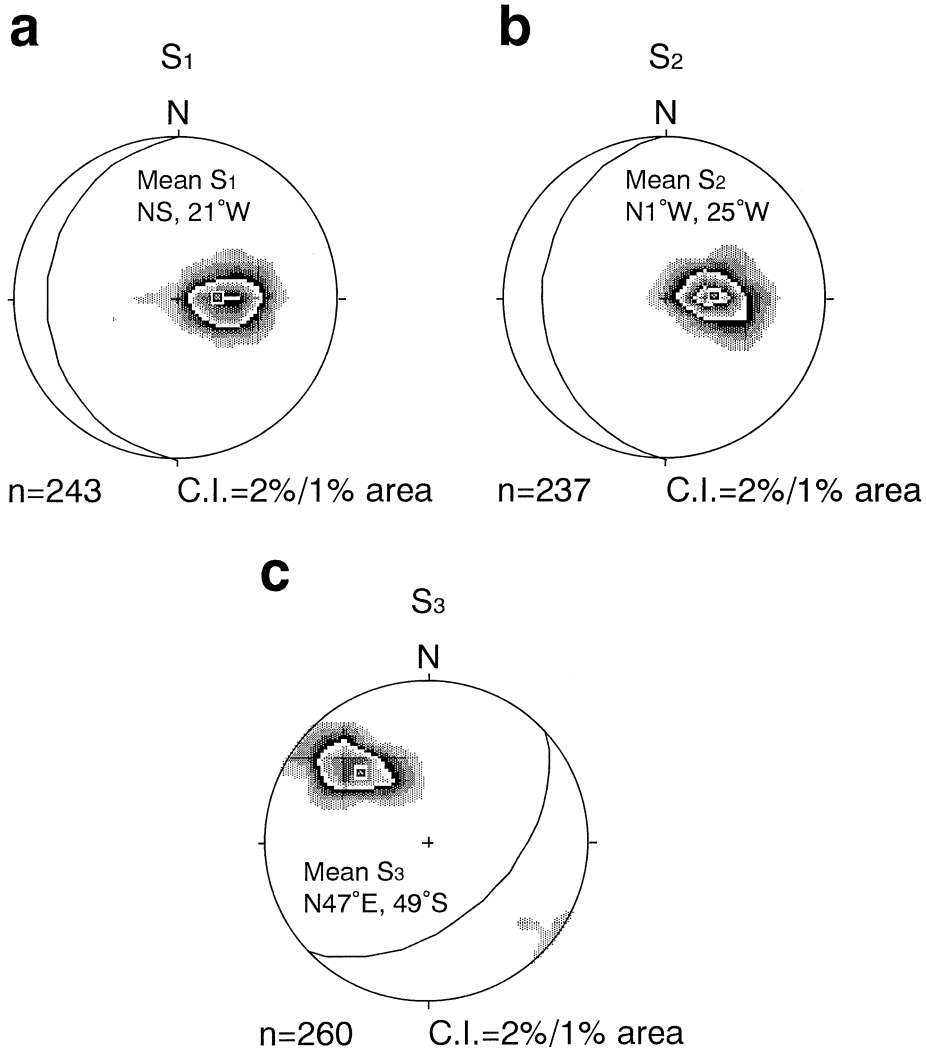

Fig. 3. Contoured stereograms of poles to (a) S_1, (b) S_2, and (c) S_3. Lower hemisphere equal-area projections are shown.

of terrigenous sedimentary rocks with rare oceanic materials such as limestone and chert (Hashimoto and Nakagawa, 1978). The eastern part of the Nago Group is composed mainly of pelitic schist, phyllite, slate, and turbidites, whereas the western part is dominated by mafic schist, pelitic schist, phyllite and lesser chert and crystalline limestone. According to Kojima et al. (1998), the eastern part of the Nago Group underwent pumpellyite–actinolite to greenschist facies metamorphism at 55–37 Ma, based on K–Ar ages of recrystallized muscovite. On the other hand, the western part suffered greenschist facies metamorphism, and K–Ar ages for recrystallized muscovite range from 77 to 61 Ma. Osozawa (1997) suggested that the boundary between the eastern and western parts of the Nago Group and the thrust fault between the Nago Group and the Kayo Formation are southeastward-verging out-of-sequence thrusts, which juxtapose different metamorphic grades. Although only trace fossils have been recovered from the Nago Group, the age of the group is generally thought to range from Cretaceous to early Eocene, based on the geotectonic framework between the Ryukyu Arc and southwest Japan and the fact that the Nago Group is in fault contact on the northwest and on the southeast with the Lower Cretaceous Motobu Group and the middle Eocene Kayo Formation, respectively. The Kayo Formation consists of coherent trench fill turbidites, which record progressive deformation during offscraping (Ujiie, H., 1989; Ujiie, K., 1997; Ujiie et al., 1997). The ancient accretionary complexes in Okinawa Island show overall younging toward the southeast (Pacific side). This geotectonic framework is modified by subvertical NW–SE striking transverse faults of both strike-slip and normal-slip components (Fig. 1b).

The study area is located along the SE margin of the Nago Group close to the contact with the Kayo Formation (Fig. 1b). Subvertical NW–SE trending faults are developed both at the northeastern and southwestern margins of the study area (Fig. 1b). Fig. 2 shows a geologic map of the coast and a cross-section of the study area. In this area, the Nago Group constitutes the sandstone–shale mélange

characterized by sandstone blocks in mudstone matrix, with local well-bedded coherent parts that are composed of alternating beds of sandstone and mudstone. The mélange blocks are both matrix-supported and locally block-supported. The sandstone–shale mélange appears to be distributed along a NW-dipping thrust fault that separates the Nago Group from the offscraped Kayo Formation.

Graded bedding and Bouma sequences are preserved in sandstones of the mélange. Therefore, coherent alternating beds of sandstone and mudstone were initially deposited as turbidites. At one place, trace fossils assigned to *Spiroraphe* have been identified on the bottom surfaces of sandstone, suggesting that the sediments were deposited in a deep-marine environment.

3. Deformation structures and processes in the mélange

D_1, D_2, and D_3 deformation phases are identified in the mélange and are characterized by structural foliations; S_1, S_2, and S_3, respectively. D_1 is defined as the deformation associated with the formation of layer-parallel extensional and asymmetric fabrics. Mud intrusions were contemporaneous with D_1. D_1 resulted in the development of S_1 that is defined by disrupted lithologic layering and layer-parallel foliation. Where primary bedding features, S_0, are preserved, they are oriented parallel to S_1. However, S_1 was locally re-oriented or folded by heterogeneous deformation in the late stage of D_1. D_2 is defined as the deformation related to the formation of S_2 planar pressure solution cleavage and brittle microfaults. S_2 is developed parallel or oblique to S_1, while microfaults cut D_1 fabrics clearly. D_3 is defined as the deformation that occurred by shortening at a low angle or subparallel to S_1 and S_2, resulting in the formation of S_3 crenulation cleavage and cylindrical upright folding of S_1 and S_2.

S_1 (not including re-oriented or folded S_1) and S_2 strike N–S and dip gently westward (Fig. 3a and b), showing a northward deviation from the general NE-strike of the Nago Group. In contrast, S_3 strikes southwestward and dips moderately to steeply southeastward (Fig. 3c). Neither major faults nor macroscopic folds with wavelength more than a few tens of meters are recognized in the mélange; strata in the mélange young west without obvious duplication, and the thickness of the mélange reaches a maximum of approximately 1.7 km.

3.1. D_1

Pinch-and-swell and boudinage structures are ubiquitously developed in sandstone blocks of the mélange, indicating the deformation resulted from layer-parallel extension. These structures define a weak but disrupted lithologic layering that is oriented parallel to the foliation defined by alignment of matrix phyllosilicates (Fig. 4a).

D_1 is locally defined by a *S–C* fabric in the mélange (Fig. 4b–g). The *S–C* fabrics are geometrically analogous to the *S*- and *C*-surfaces of mylonites in metamorphic rocks (Lister and Snoke, 1984). The shear zones that display *S–C* fabrics range in thickness from less than 1 m to more than 10 m. The upper and lower contacts of the *S–C* fabric zones are poorly defined, commonly showing transitional boundaries. The *C* surfaces within the *S–C* fabric zones range up to a few centimeters in thickness and are parallel to S_1 located outside the *S–C* fabric zones. The *C* surfaces do not show signs of brittle fracturing, implying that they reflect ductile shear (Fig. 4b). In the domains isolated by the *C* surfaces, S_1 is re-oriented at less than 45° to the *C* surfaces and is transected sharply or deflected by the *C* surfaces, showing sigmoidal shape between them (Fig. 4c). Sandstone blocks within the *S–C* fabric zones commonly exhibit asymmetrical shapes in the mudstone matrix and are locally accompanied by asymmetric tails in both outcrop and microscopic scales (Fig. 4d and e). The tails are composed of grain aggregates of sands that taper away from the sandstone blocks along the *C* surfaces. In thin sections, sand blocks are locally disaggregated asymmetrically along the *C* surfaces (Fig. 4e). Therefore, the sandstone blocks appear to have acted as partially consolidated blocks in a mudstone matrix. On the other hand, some of the sandstone blocks within the *S–C* fabric zones are disaggregated in both outcrop and microscopic scales (Fig. 4f and g).

S_1 is in places folded, showing tight to isoclinal, asymmetric and recumbent structures with wavelengths ranging from a few tens of centimeters to less than 10 m. In the well-bedded coherent parts that are preserved in the mélange, S_0 is locally asymmetrically folded (Fig. 4h). Here, both sandstone and mudstone layers are thicker at the hinge than on the limb, suggesting intergranular flow toward the hinge during folding. The most intensely deformed folds are noncylindrical in shape, probably tending towards sheath folds. In this case, the fold axes and axial surfaces are curvilinear and curviplanar, respectively.

Mud intrusions are locally developed with D_1 fabrics and are commonly crosscut by the S_2 pressure solution cleavage and the microfaults associated with D_2. They are identified by the fact that the preexisting alignment of sandstone blocks is modified and/or destroyed, commonly associated with the disruption and disaggregation of sandstone by mud injections (Fig. 4i). During intrusion of muds, the sandstone blocks were deformed heterogeneously, possibly depending on differences in degree of their cohesion and lithification. Some sandstone blocks within the mud intrusions exhibit irregular external shapes and are chaotically mixed with mudstone matrix (Fig. 4j), suggesting that sandstone blocks were weakly cohesive and were disaggregated. In the extreme case, disaggregation in sandstone blocks becomes complete, locally making a sandy mudstone matrix with a light grayish color. In contrast, other sandstone blocks within the mud intrusions preserve distinct external shapes. In such a case, the interfaces between the sandstone blocks and injected muds are planar, and some sandstone fragments appear to have been separated from the adjacent sandstone

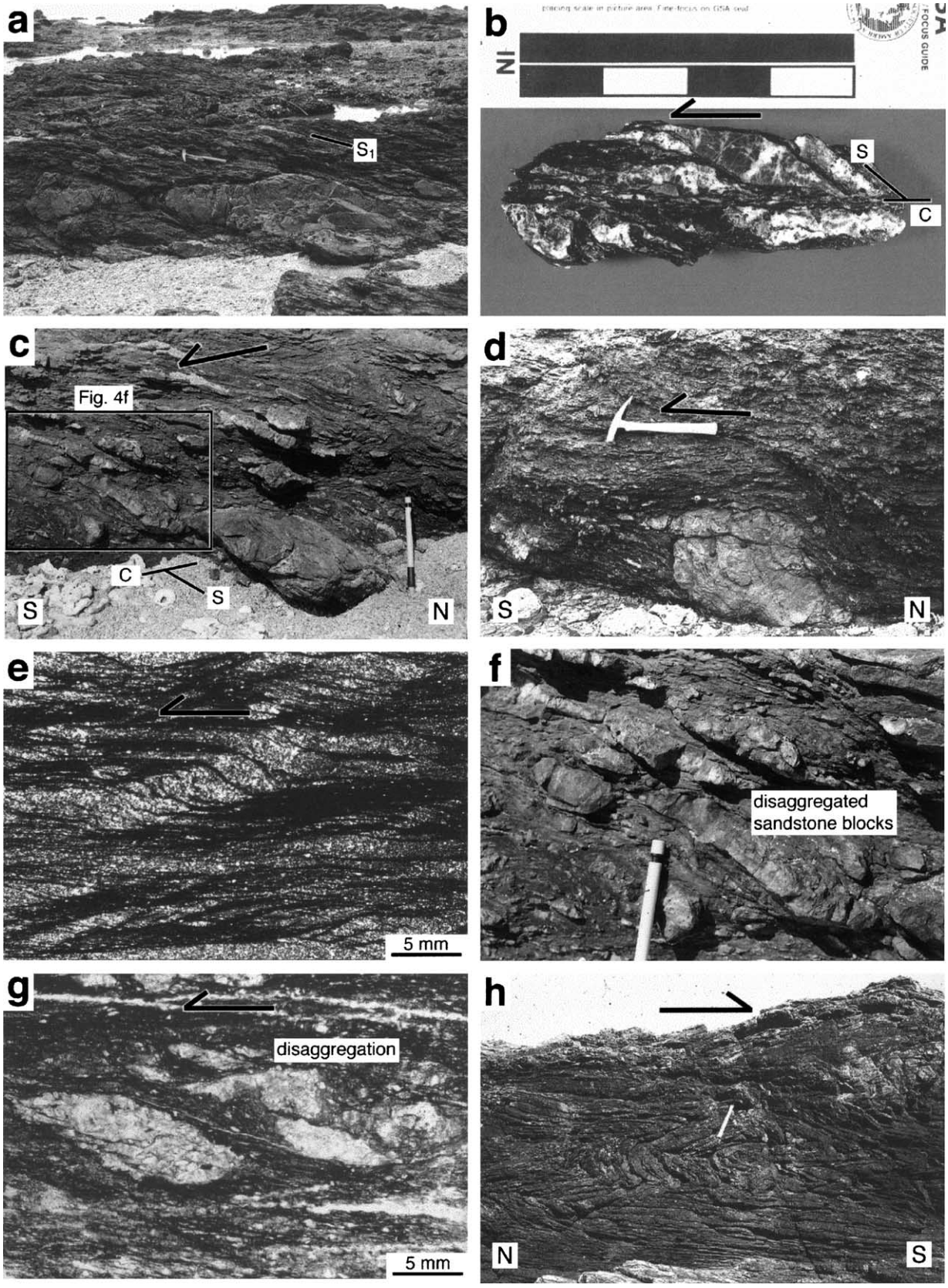

Fig. 4. D_1 structures. Arrows indicate the sense of shear. (a) Pinch-and-swell structures and boudinage that are oriented parallel to S_1. *S–C* fabrics (b) on polished surface and (c) on outcrop. (d) and (e) The sandstone blocks with asymmetric tails. (f) *S–C* fabric with disaggregation. (g) Photomicrographs of *S–C* fabric. Note the disaggregated sandstone inclusion in the right part. (h) Asymmetric folds in thin-bedded turbidites of the coherent part. (i) Sandstone blocks disrupted and disaggregated by mud injections. (j) Sandstone blocks within mud intrusions display irregular external shapes and chaotically mixed with the mudstone matrix. (k) Photomicrograph of mud injection. Note the sharp and planar interfaces between injected parts and the surrounding sandstone block.

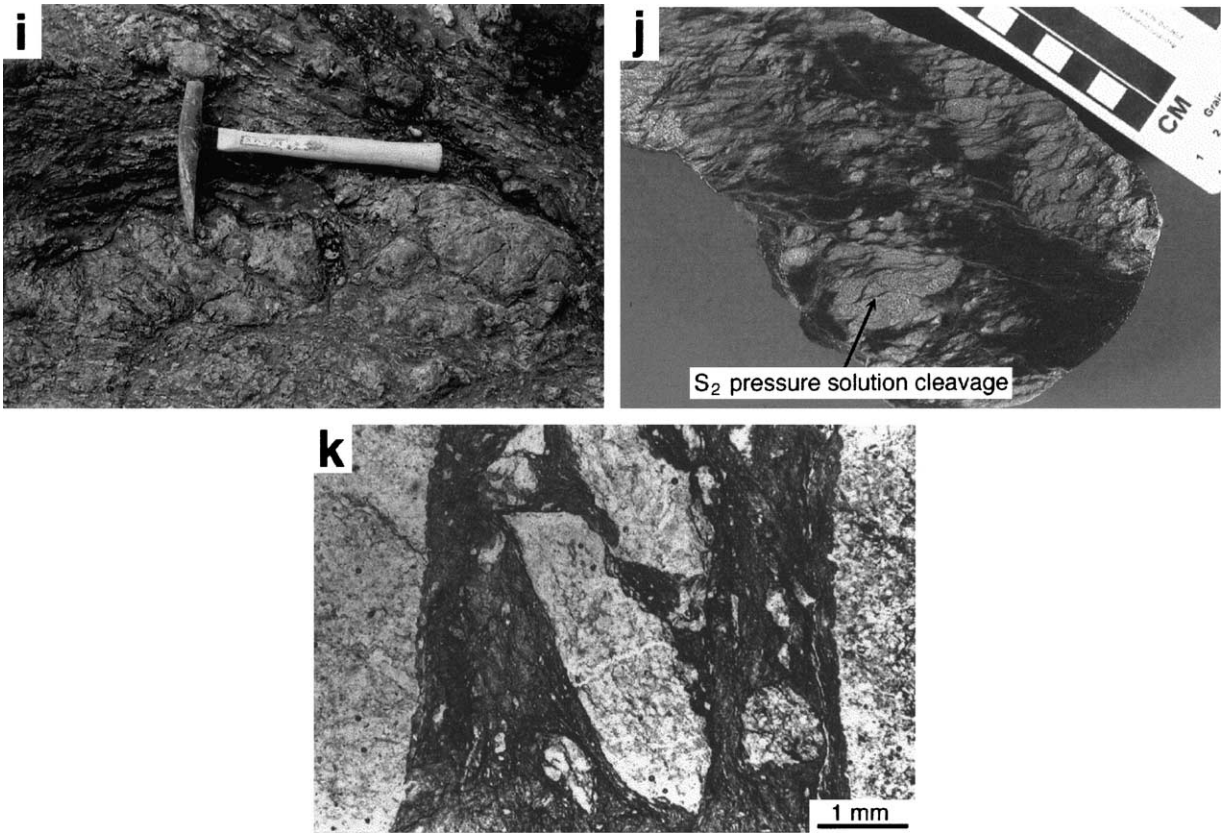

Fig. 4. (*continued*)

blocks and incorporated into injected muds (Fig. 4k). These features suggest that sandstone blocks were cohesive and were not disaggregated.

The overall result of D_1 was the development of alternation of asymmetric and layer-parallel extensional fabrics in the mélange; asymmetric fabrics are represented by *S–C* fabrics and asymmetric folds whereas extensional fabrics are shown by boudined layers that are parallel to S_1. Deformation features of D_1 structures suggest that the dominant deformation mechanism was independent particulate flow (Borradaile, 1981) and mechanical rotation with grain boundary sliding, which dominates in poorly lithified sediments (Knipe, 1986). Mud intrusions indicate that the mud, which intrudes the mélange, was overpressured during D_1.

3.2. D_2

The S_2 pressure solution cleavage is well developed in the upper structural level of the mélange and gradually decreases in intensity toward the lower structural level (Fig. 2). S_2 overprints the asymmetric and layer-parallel extensional fabrics that were formed during D_1; S_2 cuts S_1 in asymmetric fabric zones where S_1 is re-oriented or folded, while it is parallel to S_1 in layer-parallel extensional fabric zones. S_2 commonly crosscuts the D_1 structures, which formed in association with intrusion of muds and disaggregation of sandstone (Fig. 4j). On the microscopic scale, S_2 is defined by pressure solution seams of abundant, dark insoluble material and aligned and/or recrystallized phyllosilicates. Quartz grains are flattened parallel to the cleavage domains, and material that was dissolved during cleavage formation has been precipitated adjacent to resistant grains in strain shadows. These observations indicate that the upper structural level of the mélange suffered layer-perpendicular flattening.

Microfaults are developed both in sandstone blocks and the mudstone matrix. Microfaults were formed during D_2 and thus were synchronous with S_2 pressure solution cleavage, because they displace D_1 fabrics and are deflected by D_3 folds. In contrast to the case of S_2, microfaults gradually increase their intensities toward the lower structural level of the mélange (Fig. 2). Many of the microfaults in sandstone blocks are sharp, planar and continuous (Fig. 5a), and in places merge with or branch from one another. Microfaults commonly cut quartz veins and mud injections, with displacements of up to 1 cm (Fig. 5b). On the surface of the sandstone blocks, individual microfaults are defined as linear scars that are less than a few millimeters in width and parallel or subparallel to one another, showing mullion-like features. Sandstone blocks deformed by microfaults have been disaggregated into smaller clasts and scattered into the mudstone matrix (Fig. 5b). In thin sections, microfaults in sandstone blocks are generally represented by dark insoluble material showing pressure solution and

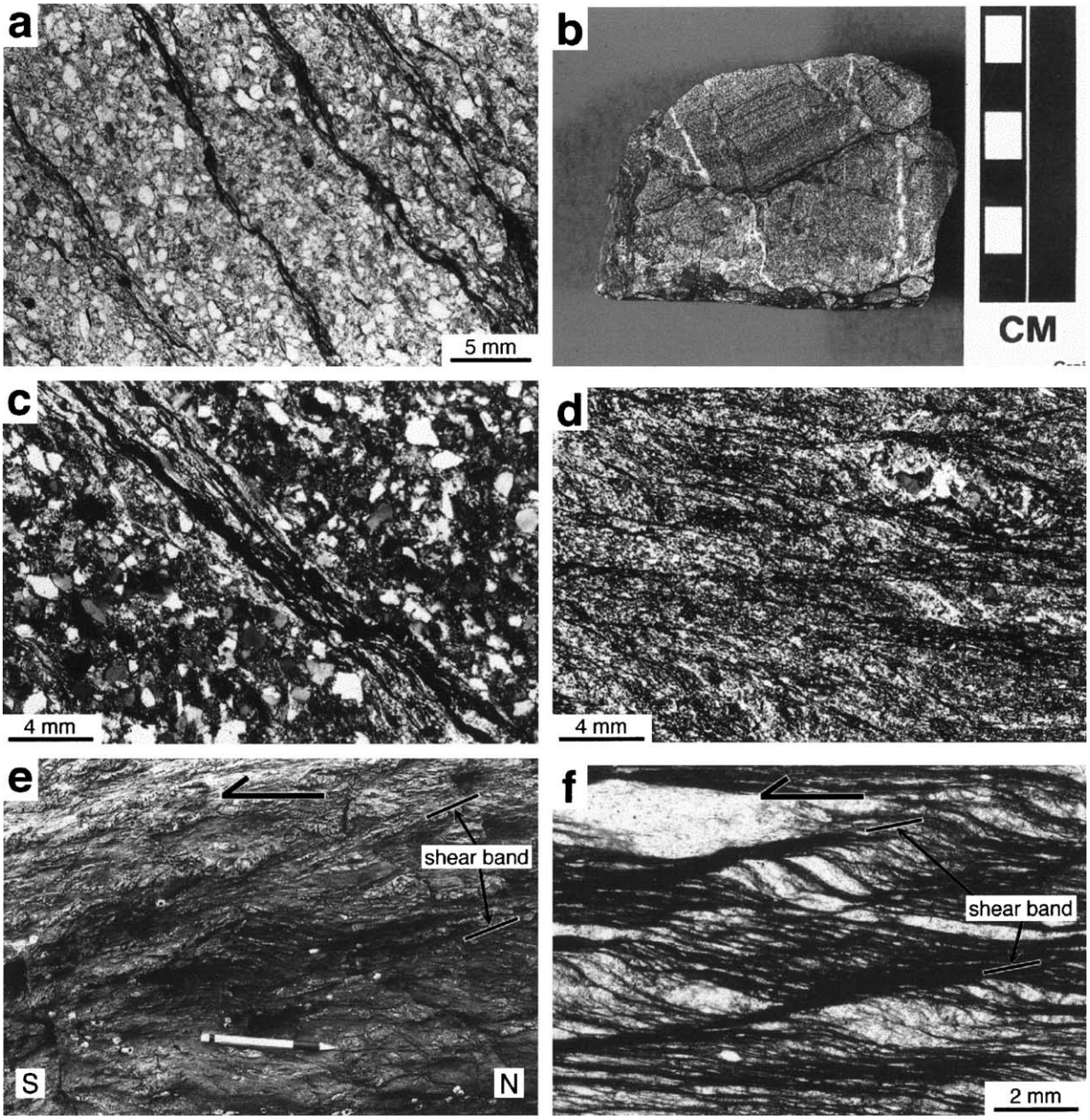

Fig. 5. D_2 structures. Arrows indicate the sense of shear. (a) Microfaults in sandstone blocks. (b) Microfaults on polished surface of a sandstone block. Quartz veins were displaced by microfaults, and a sandstone block was disaggregated along a microfault at its margin. (c) Photomicrographs of a microfault in sandstone block. (d) Microfaults in mudstone matrix. (e) Extensional shear bands on outcrop. (f) Photomicrographs of extensional shear bands.

preferentially oriented and/or recrystallized phyllosilicates trending parallel to fault surfaces (Fig. 5c). Grain breakage is commonly recognized along the margins of microfaults. Locally, asymmetrical shear foliation or clasts are recognized within the microfaults. On the other hand, microfaults in the mudstone matrix are characterized by polished surfaces, in places with striations. On a microscopic scale, they are defined by the complex network of surfaces that are filled with dark insoluble materials showing pressure solution (Fig. 5d). These faults cross-cut grains in the mudstone matrix and also cut D_1 asymmetric fabric elements. In places, some isolated fragments of grains in the mudstone matrix have been entrained within microfaults. These observations illustrate that brittle shear permeated the lower structural level of the mélange.

The extensional shear bands are rarely observed (Fig. 5e and f). They commonly transect S_1 and S_2 at low angles but are cut by S_3 crenulation cleavages (described later). The extensional shear bands displace and drag D_1 fabrics, and cut the sandstone blocks that were injected by muds during D_1. Thus, the shear bands are considered to be D_2 structures. In thin sections, the aligned phyllosilicates and dark insoluble materials produced by pressure solution are concentrated along the shear bands (Fig. 5f).

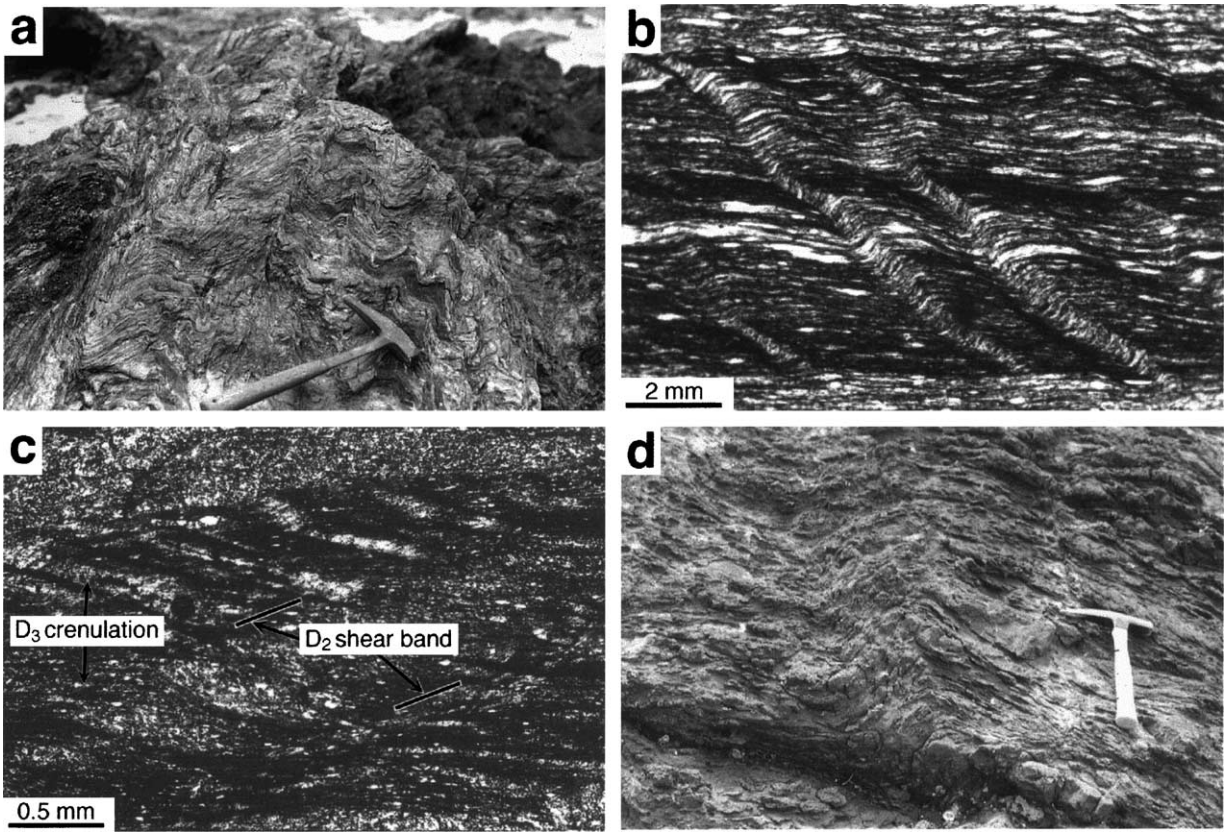

Fig. 6. D_3 structures. Crenulation folds (a) on outcrop and (b) in thin section. (c) Relationship between D_2 fabrics and D_3 crenulation cleavages. (d) Cylindrical upright fold formed in disrupted lithologic layering.

To summarize, D_2 is represented by the partitioning of deformation in the mélange in which brittle shear and layer-perpendicular flattening progressed in the lower and upper structural levels, respectively. On the other hand, the rarely observed shear bands suggest that shear localization also occurred at some stage of D_2. During D_2, the sediments in the mélange were lithified, and deformation by pressure solution became dominant.

3.3. D_3

Crenulations and S_3 crenulation cleavage are preferentially developed in the upper structural level of the mélange where S_2 pressure solution cleavage is well developed. On a microscopic to mesoscopic scale, crenulations are defined by folding of older S_2 (Fig. 6a and b). The crenulations show symmetric forms characterized by large amplitude with respect to wavelength or normal and reverse asymmetries. S_3 is generally inclined moderately or is normal to S_1 and S_2. In thin section, S_3 is represented by dark insoluble material showing enhanced pressure solution and forms a distinct fabric with microlithons that accompanies various degrees of folding of S_1 and S_2. Locally, S_3 was preferentially formed where D_2 extensional shear bands and the oriented phyllosilicates were concentrated resulting in folding, reorienting, and close spacing of phyllosilicates (Fig. 6c). S_3 commonly occurs at high angles to the shear bands and clearly cuts them. In places, however, S_3 is subparallel to the extensional shear bands. In this case, S_3 is distinguished from shear bands by: (1) the angles between S_2 and S_3 being generally higher than those between S_2 and the shear bands; (2) the folds of S_2 between S_3 have larger amplitude than those between the shear bands; and (3) in contrast to shear bands that accommodate extension of S_2, S_3 displays apparent shortening of S_2.

Cylindrical upright folds with wavelength up to 1 m are locally recognized in the mélange, accompanying the folding of S_1 and/or S_2. The axial surfaces of these folds are moderately inclined to perpendicular with respect to S_1 and S_2. Generally, where S_3 crenulation cleavage is adjacent to upright folds, the axial surfaces of the folds are parallel to the cleavage surface. Cylindrical upright folds are best developed in well-cleaved mudstone, and they occur locally in the disrupted lithological layering. In the latter case, folds are defined by isolated hinges and limbs composed of oriented, disrupted sandstone blocks (Fig. 6d).

As a whole, the deformation features of D_3 indicate that the mélange experienced shortening subparallel to S_1 and S_2 during D_3. The degree of development of D_3 fabrics was strongly affected by the presence of S_2 pressure solution cleavage, and thus D_3 occurred heterogeneously in the mélange.

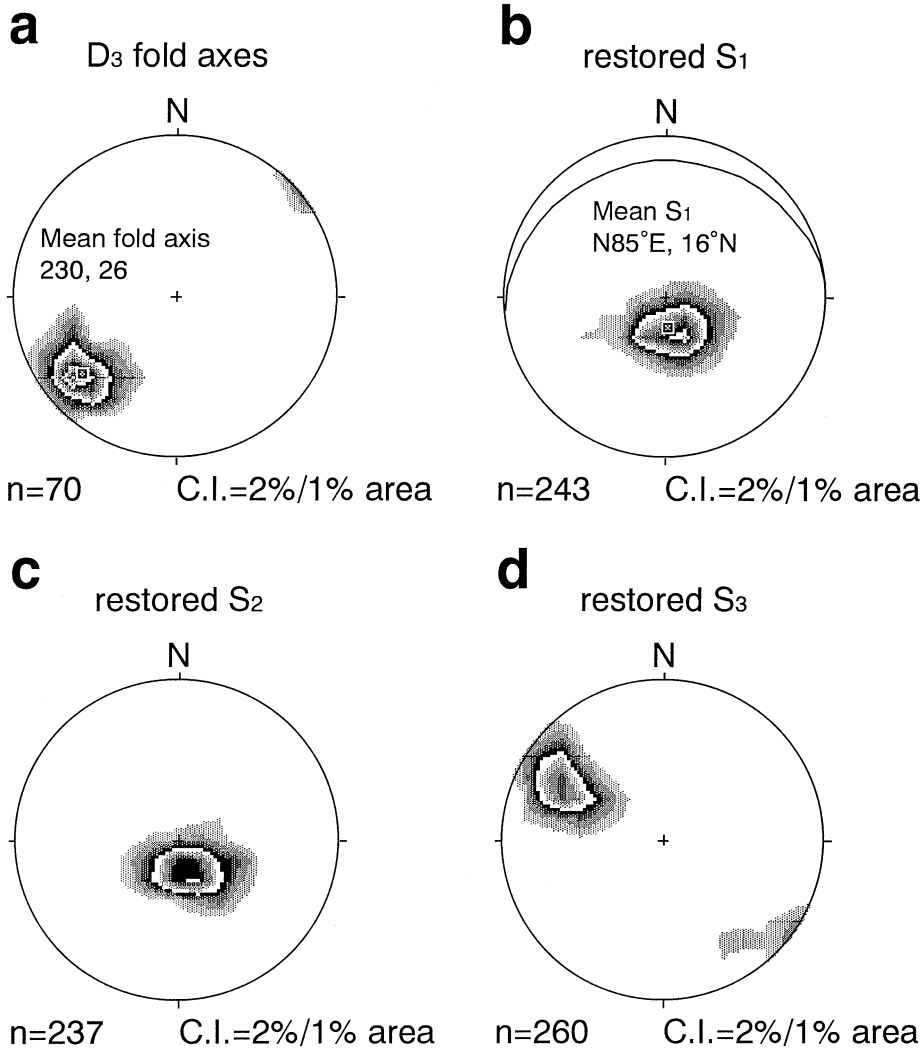

Fig. 7. (a) Attitudes of D_3 fold axes. Contoured stereograms of poles to (b) S_1, (c) S_2, and (d) S_3 after rotation of D_3 fold axes is removed. Lower hemisphere equal-area projections are shown.

4. Kinematics of the mélange

In an accretionary prism, progressive imbrication and related tilting could occur during development of mélange, and mélange fabrics may be formed during and/or after strata were rotated into a steep attitude (e.g. Kusky and Bradley, 1999). Alternatively, mélange fabrics may develop along décollement zones or within slope sediments where strata are poorly lithified and are subhorizontal (e.g. Cowan, 1982; Fisher and Byrne, 1987; Kimura and Mukai, 1991). As shown in Figs. 2 and 3, strata in the mélange have not been rotated to steep attitude. The D_1 deformation features indicate that the sediments in the mélange were poorly lithified, suggesting that D_1 took place immediately after deposition. Strata in the mélange are thus considered to have been subhorizontal during D_1. Therefore, the tilting correction is necessary to restore the kinematics of D_1 to the appropriate original attitude.

As in the case of paleocurrent analysis, rotation of the regional axis of plunge of fold about horizontal axis perpendicular to the trend of fold axis was performed before the tilting correction. In the study area, most of the D_3 fold axes plunge to the SW, and mean D_3 fold axis trends 230 and plunges 26, suggesting the regional angle of plunge (Fig. 7a). Therefore, the following geometric correction was carried out: the data was rotated 26° clockwise about a NW-trending horizontal axis (320, 0) so the D_3 fold axes are horizontal. The restored S_1 and S_2 strike E–W to ENE–WSW and dip gently northward, whereas the restored S_3 strikes NNE–SSW to NE–SW and dips moderately to steeply southeast (Fig. 7b–d). After correction about the rotation of fold axes, S_1 foliations oriented parallel to bedding were rotated to horizontal.

Lower hemisphere equal-area projections of restored D_1 structural data are shown in Fig. 8. The axes defined by the pinch-and-swell necks are mostly horizontal and E–W trending (Fig. 8a). Quartz veins developed in the most extended parts of pinch-and-swell and boudinage strike

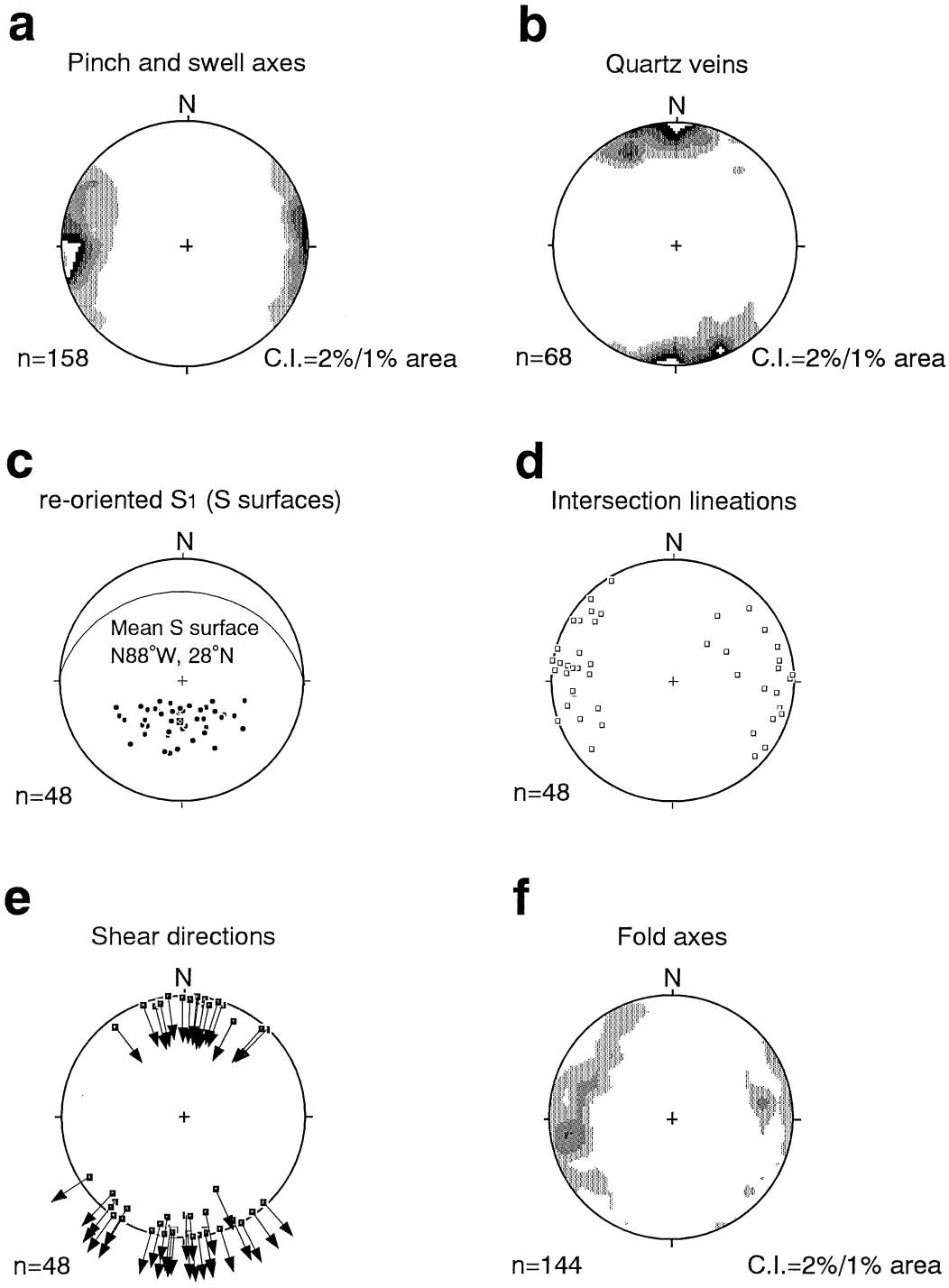

Fig. 8. Structural data from the D_1 structures after restorations (see text for further explanation). Lower hemisphere equal-area projections are shown. (a) Attitudes of pinch and swell axes. (b) Poles to quartz veins in the neck regions of pinch-and-swell and boudinage structures. (c) Poles to re-oriented S_1 (*S* surfaces) in the *S*–*C* fabrics. (d) Attitudes of intersection lineations between *C* and *S* surfaces. (e) Shear directions determined from the *S*–*C* fabrics. (f) Attitudes of fold axes.

approximately east–west and dip almost vertically (Fig. 8b). These results suggest N–S trending subhorizontal extension during D_1. The asymmetric fabrics within the *S*–*C* fabric zones provide the sense of shear. The *C* surfaces are generally subhorizontal after restoration. In contrast, the poles to re-oriented S_1 (*S* surfaces) display a broad scatter with a strong, steep south-plunging maximum (Fig. 8c). The intersection lineations between *C* and *S* surfaces are dominantly E–W trending (Fig. 8d). The shear directions were obtained based on the assumption that they are perpendicular to intersection lineations on the shear surfaces (e.g. Kano et al., 1991; Onishi and Kimura, 1995; Kusky and

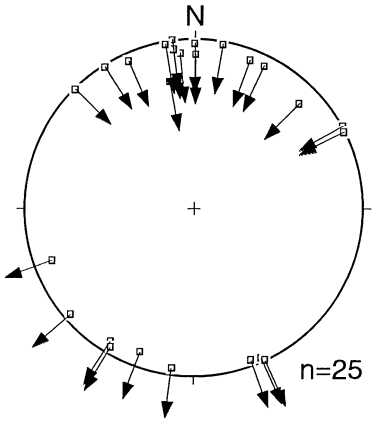

Fig. 9. Lower hemisphere equal-area projection of D_2 shear directions after restorations.

Bradley, 1999). The asymmetry of the *S–C* fabric zones suggest southward-directed shearing (Fig. 8e). This is consistent with the fact that D_1 asymmetric and cylindrical folds exhibit a consistent *Z* geometry when viewed to the east, and the restored fold axes are dominantly E–W trending and horizontal (Fig. 8f). On the other hand, the axes of noncylindrical folds tend to plunge northwest or north-northwest.

During D_2, S_2 pressure solution cleavage was formed by layer-perpendicular flattening. Except for the asymmetric fabric zones where S_1 is re-oriented or folded, S_2 is developed parallel to S_1. Thus, strata were considered to be largely subhorizontal during D_2. D_2 kinematic indicators are relatively rare. The slip directions of microfaults are not generally known because the surfaces of the faults are not exposed. However, as in the case of D_1 asymmetric fabrics within the *S–C* fabric zones, D_2 extensional shear bands can be used as a shear-sense criterion. In outcrop, the shear bands indicate a southward-directed shear. Fig. 9 shows shear directions determined from shear bands after restorations. The restored shear directions suggest dominantly southward-directed shearing. Therefore, D_2 appear to be kinematically similar to D_1.

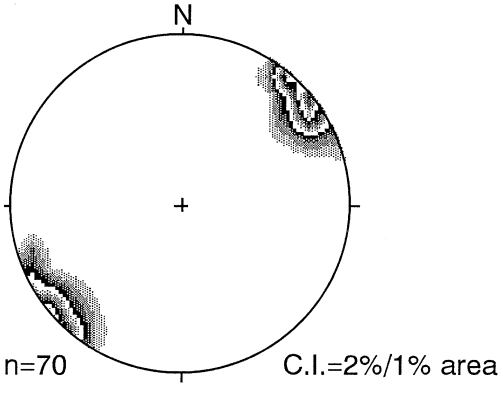

Fig. 10. Attitudes of D_3 fold axes after rotation of D_3 fold axes is removed. Lower hemisphere equal-area projection is shown.

D_3 occurred by shortening subparallel to S_1 and S_2. Thus, the mélange records a change in the geometry of deformation from D_2 to D_3. Temporal relationships between D_3 and rotation of D_3 fold axes are unclear. If rotation of D_3 fold axes occurred after D_3, D_3 fold axes should be corrected. The restored D_3 fold axes are NE–SW trending (Fig. 10) and are subparallel to both the strike of S_3 and D_3 fold axes before correction (Fig. 7a and d). Thus, D_3 is considered to record NW-directed shortening.

5. Discussion

5.1. Spatial distribution and temporal progression of décollement-related deformation

Initial D_1 in the mélange is characterized by subhorizontal layer-parallel extension, resulting in the development of boudined layers that are arranged parallel to S_1 layer-parallel foliation (Fig. 4a). Generally, subhorizontal layer-parallel extension in mélanges has been explained by two models: one is gravity-driven slumping or sliding of surficial slope sediments that cover the prisms (e.g. Cowan, 1982), the other is associated with layer-parallel shear during the vertical loading that occur in sediments in and below décollement (e.g. Fisher and Byrne, 1987; Brown and Behrmann, 1990; Kusky and Bradley, 1999). In the latter case, vertical loading is due to the wedge geometry of the overriding accretionary prisms. The sediments in the mélange of the study area were initially deposited as turbidites, which are uncommon in slope sediments on accretionary prisms (e.g. Taira and Ashi, 1993). In addition, D_1 layer-parallel extensional fabrics and the associated kinematics are systematic, suggesting that they resulted from a tectonic process. Therefore, D_1 is interpreted to occur in the footwall of the décollement, reflecting layer-parallel shear in conjunction with flattening due to the vertical loading during underthrusting (Fig. 11a).

Subsequently, S_1 and boudined layers were locally re-oriented or folded by southward-directed shearing, resulting in the development of *S–C* fabrics (Fig. 4b–g) and asymmetric folds. These asymmetric fabrics alternate with layer-parallel extensional fabrics that were formed during D_1 (Fig. 11b). These features strongly suggest that the asymmetric fabrics result from heterogeneous bulk shear in the mélange. The locally observed noncylindrical folds probably reflect the high shear strain zones. Consequently, I propose that when underthrusting progressed, deformation in the footwall of the décollement evolved from subhorizontal, layer-parallel extension to heterogeneous shear (Fig. 11). Similar layer-parallel extensional and asymmetric fabrics were also described from other mélanges in accretionary complexes (e.g. Fisher and Byrne, 1987; Kano et al., 1991; Onishi and Kimura, 1995; Kusky and Bradley, 1999). Thus many mélanges may have experienced a common deformation process during underthrusting;

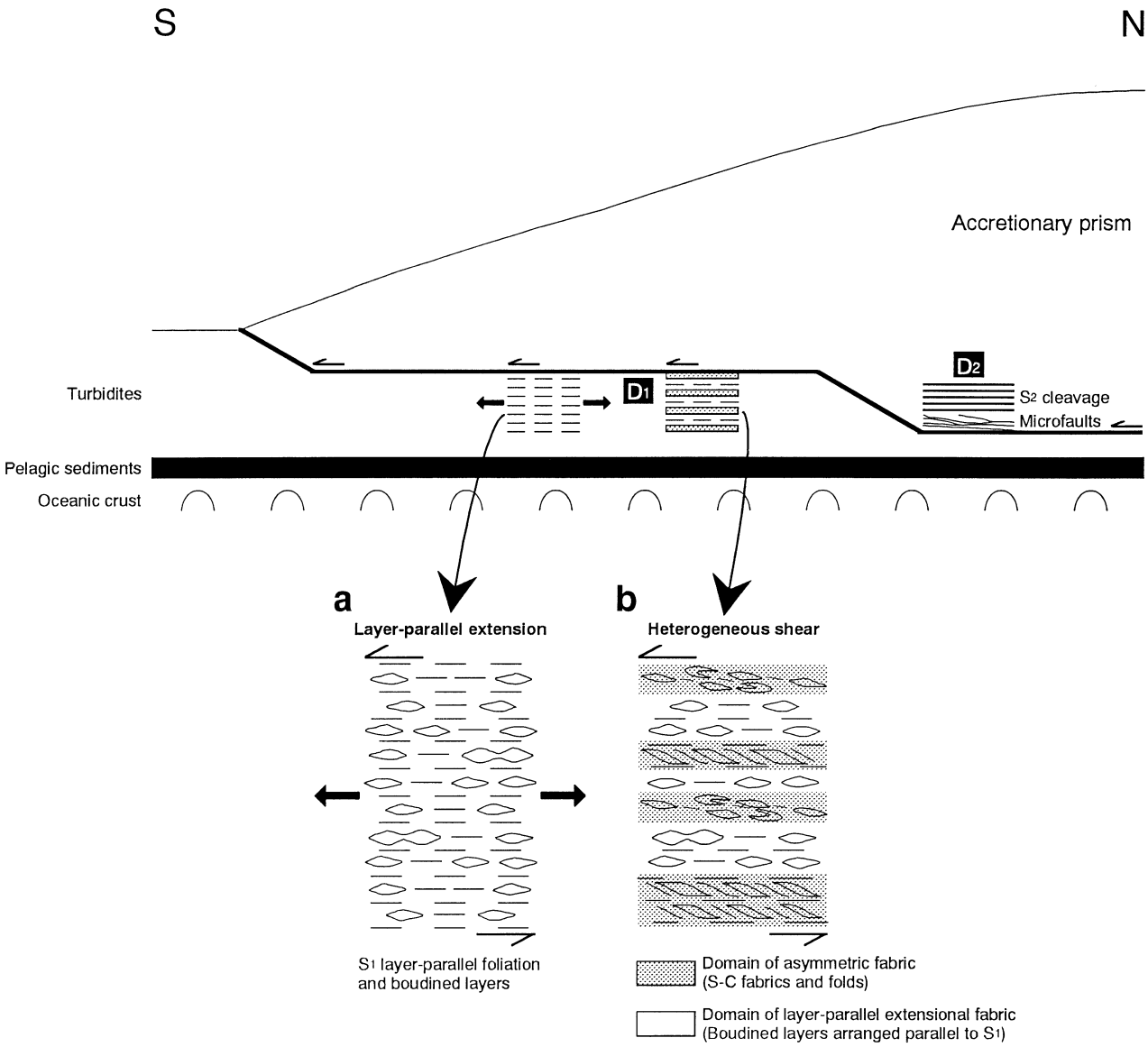

Fig. 11. A schematic model showing the spatial distribution and temporal progression of décollement-related deformation, based on structural analysis of the mélange in the Shimanto accretionary complex (modified after Ujiie et al., 2000).

deformation by subhorizontal layer-parallel extension followed by heterogeneous shear.

The development of D_1 extensional and asymmetric fabrics was probably accompanied by pore size reduction and related fluid expulsion, leading to consolidation in the footwall of the décollement. On the other hand, mud intrusions commonly cut and disturb the preexisting D_1 fabrics (Fig. 4i–k). This relation suggests that fluid was supplied to the consolidated portions characterized by extensional and asymmetric fabrics and that the footwall of the décollement was in places overpressured. The fluid may have been transported from deeper sources as a result of clay dehydration and hydrocarbon generation (Moore and Vrolijk, 1992). High fluid pressure is likely in the footwall of the décollement because it is buried rapidly (more than 20 km/my) before dewatering (e.g. Fisher and Byrne, 1987; Moore, 1989).

During D_2, the upper structural level of the mélange experienced pervasive layer-perpendicular flattening represented by S_2 planar pressure solution cleavage (Fig. 2). In contrast, the lower structural level was permeated by microfaulting related to brittle shear (Figs. 2 and 5a–d). Such differences in deformation style have constrained the degree of S_3 development in the mélange (Fig. 2). One possibility for the partitioning of D_2 deformation in the mélange is that it may be related to rheological differences between the lower and upper structural levels, which are controlled by bulk composition and anisotropy (e.g. sand–mud ratio). However, this scenario is unlikely, because: (1) the mélange is composed of monotonous lithologies (turbidites), and (2)

various sand–mud ratio arises in each structural level of the mélange.

Alternatively, differences in deformation at different structural levels could reflect proximity to the basal décollement that developed beneath the mélange, and D_2 may occur in the hanging wall of the décollement (Fig. 11). For example, shear strain could have been concentrated in the lower structural level of the mélange due to proximity to the underlying décollement. In this case, the lower structural level would be pervasively sheared, while the upper structural level would not. The partitioning of deformation in the mélange is also recorded in magnetic fabrics (Ujiie et al., 2000). The magnetic fabrics of the upper structural level of the mélange intensify with the development of S_2 pressure solution cleavage, reflecting the incremental strain geometries associated with D_2. In the lower structural level, however, penetrative strain related to D_2 rarely modified the preexisting magnetic fabrics that document D_1 strain geometries, because during D_2, shear strain was accommodated by brittle microfaults, which are a volumetrically minor component of the lower structural level. These features indicate that the décollement-related shear evolved from heterogeneous bulk shear during D_1 to shear concentration in the lower structural level of the mélange during D_2 (Fig. 11). Change in deformation style from D_1 ductile shear to D_2 brittle shear may be dependent on the progression of lithification of the sediments and/or the change in physical parameters such as strain rate.

Principal shortening direction during D_2, however, was subvertical in the upper structural level of the mélange, because S_2 is parallel to S_1 in zones of layer-parallel extensional fabrics. Thus the upper structural level of the mélange may have undergone flattening associated with the vertical loading of the overriding prism, and the extensional shear bands may reflect subhorizontal layer-parallel extension related to this vertical loading (Fig. 5e and f). In this case, D_2 was unlikely to occur in the hanging wall of the décollement, yet shear is concentrated in the lower structural level of the mélange. One explanation for these phenomena is that D_2 may represent the precursor for accretion of mélange beneath the overlying accretionary prism (incipient underplating): shear concentration in the lower structural level of the mélange reflects initiation of décollement propagation from shallow structural level to deeper one, whereas upper structural level suffered subvertical shortening. At the northern Barbados convergent margin, the proto-décollement is characterized by small-scale faults and extensional mud-filled veins seaward of deformation front but material above the proto-décollement appears to lack evidence for prism-related compressive stress (Moore, 2000). The mélange would be rotated to landward during the underplating after D_2, resulting in gently dipping S_1 and S_2 (Fig. 7b and c). The low dip angles of D_1 and D_2 structures might reflect the flat part of a duplex structure, because moderately- to steeply-dipping fabrics are commonly expected at ramps (e.g. Boyer and Elliott, 1982).

5.2. Relationship between mélange kinematics and plate convergence vector

There have been numerous attempts to correlate mélange kinematics with plate convergence vector (e.g. Kano et al., 1991; Onishi and Kimura, 1995; Kusky and Bradley, 1999). Shearing during D_1 was dominantly toward the south, as it was during D_2 (Figs. 8 and 9). Engebretson et al. (1985) demonstrated that the convergence vector between the Eurasia and Pacific plates rotated clockwise from northwest to north at ca. 50–55 Ma. The north-directed subduction of the Pacific plate during early Eocene is consistent with southward-directed shearing in the mélange. Therefore, the D_1 and D_2 kinematics might record the relative plate motion during early Eocene.

However, the strike of the mélange in the study area is deflected from the regional NE strike of the Nago Group. This may reflect a rotation of rocks in the study area that may occur by intra-arc block rotation related to the opening of the Okinawa Trough backarc basin since the Pleistocene (e.g. Ujiie, H., 1994). Subvertical NW–SE striking faults at the northeastern and southwestern margins of the study area and rotation of D_3 fold axes might accommodate such rotation. Without precise kinematic and paleomagnetic data about intra-arc block rotation, the D_1 and D_2 kinematic data cannot be restored to their appropriate attitudes. If rotation of D_3 fold axes postdated D_1 and D_2, however, the shear directions during D_1 and D_2 were nearly perpendicular to the strike of the mélange (Figs. 7–9). This could reflect the nearly normal subduction of the Kula plate during early Tertiary that was inferred until ca. 43 Ma (Byrne and DiTullio, 1992).

5.3. Post-accretion deformation

D_3 is represented by NNE–SSW to NE–SW striking S_3 crenulation cleavage and NE–SW trending cylindrical upright folds that were formed by shortening subparallel to S_1 and S_2. Considering that S_1 and S_2 are inferred to have been nearly horizontal during D_2 and that the maximum principal compressive stress is commonly subhorizontal in accretionary prisms (Davis et al., 1983), D_3 is interpreted to record subhorizontal intra-prism shortening, after the mélange was incorporated into the accretionary prism. The D_3 shortening direction is dominantly NW-directed, consistent with that of the middle Eocene Kayo Formation (Fig. 1b), which records seaward (southeastward) verging imbrication by offscraping accretion (Ujiie, K., 1997). Thus, if intra-arc block rotation has not taken place, D_3 can be interpreted as a response to accretion of the seaward Kayo Formation during the middle Eocene.

6. Conclusions

The mélange in the Shimanto accretionary complex of

Okinawa Island illustrates the spatial distribution and temporal progression of décollement-related deformation. During underthrusting, deformation in the footwall of the décollement progressed first by subhorizontal layer-parallel extension and then by heterogeneous ductile shear of partially lithified sediments. The overall result of these D_1 deformations is the development of alternation of asymmetric and layer-parallel extensional fabrics in the mélange. The timing relationships between mud intrusions and other structures suggest local generation of high fluid pressure in the footwall of a décollement.

Late deformation (D_2) of the mélange was characterized by the partitioning of deformation with shear concentration in the lower structural level and layer-perpendicular flattening in the upper structural level of the mélange. These differences appear to reflect the proximity to the underlying décollement, and late deformation was inferred to occur in the hanging wall of the basal décollement. In this stage, décollement-related shear is accomplished by brittle microfaulting, probably dependent on increased lithification and/or change in physical parameters (e.g. strain rate) in the mélange.

The kinematics of décollement-related deformation suggest that they may reflect the relative plate motion during early Tertiary. The mélange suffered subhorizontal shortening after it was incorporated into the accretionary prism, resulting in the formation of crenulation cleavage and cylindrical upright folds (D_3). In this process, the degree of structural development was strongly affected by the previous fabrics, which were formed during late décollement-related deformation that took place in the hanging wall of the décollement.

Acknowledgements

I express my sincere appreciation to Wonn Soh and Gaku Kimura for their instructive suggestion during the study. J. Casey Moore and Ken-ichi Kano are greatly appreciated for many thoughtful comments on early drafts of the paper. The paper benefited from critical and helpful reviews by Jon Lewis, Timothy M. Kusky, Donald Fisher and an anonymous reviewer. Finally, special thanks to Yujiro Ogawa for helpful comments and insights during various stages of the study. This study was supported by the Fukada Geological Institute, the Fujiwara Natural History Foundation, and the JSPS Research Fellowship award to the author.

References

Borradaile, G.J., 1981. Particulate flow of rock and the formation of cleavage. Tectonophysics 72, 305–321.

Boyer, S.E., Elliott, D., 1982. Thrust systems. Bulletin of the American Association of Petroleum Geologists 66, 1196–1230.

Brown, K.M., Behrmann, J.H., 1990. Genesis and evolution of small-scale structures in the toe of the Barbados Ridge accretionary wedge. Proceedings of the Ocean Drilling Program Scientific Results 110, 229–244.

Byrne, T., DiTullio, L., 1992. Evidence for changing plate motions in southwest Japan and reconstructions of the Philippine Sea plate. The Island Arc 1, 148–165.

Cowan, D.S., 1982. Deformation of partly dewatered and consolidated Franciscan sediments near Piedras Blancas Point, California. In: Leggett, J.K. (Ed.). Geological Society of London Special Publication, vol. 10, pp. 439–457.

Davis, D., Suppe, J., Dahlen, F.A., 1983. Mechanics of fold-and-thrust belts and accretionary wedges. Journal of Geophysical Research 88, 1153–1172.

DiTullio, L., Byrne, T., 1990. Deformation paths in the shallow levels of an accretionary prism: the Eocene Shimanto belt of southwest Japan. Geological Society of America Bulletin 102, 1420–1438.

Engebretson, D., Cox, A., Gordon, R.G., 1985. Relative motions between oceanic and continental plates in the northern Pacific basin. Geological Society of America Special Publication 206, 1–59.

Fisher, D., Byrne, T., 1987. Structural evolution of underthrusted sediments, Kodiak Island, Alaska. Tectonics 6, 775–793.

Hashimoto, S., Nakagawa, H., 1978. Geology of the northern part of Okinawa-jima. In: Kizaki, K. (Ed.). Geological Studies of the Ryukyu Islands, vol. 3, pp. 23–29.

Kano, K., Nakaji, M., Takeuchi, S., 1991. Asymmetrical mélange fabrics as possible indicators of the convergent direction of plates: a case study from the Shimanto Belt of the Akaishi Mountains, central Japan. Tectonophysics 185, 375–388.

Karig, D.E., 1986. Physical properties and mechanical state of accreted sediments in the Nankai Trough, Southwest Japan Arc. Geological Society of America Memoir 166, 117–133.

Kimura, G., Mukai, A., 1991. Underplated units in an accretionary complex: mélange of the Shimanto Belt of eastern Shikoku, southwest Japan. Tectonics 10, 31–50.

Knipe, R.J., 1986. Deformation mechanism path diagrams for sediments undergoing lithification. Geological Society of America Memoir 166, 151–160.

Kojima, T., Nishimura, Y., Takami, M., Itaya, T., 1998. Metamorphism and K–Ar ages of Nago Formation, Okinawa Islands. Proceedings of the Nishinihon Branch of the Geological Society of Japan 113, 27.

Kusky, T.M., Bradley, D.C., 1999. Kinematic analysis of mélange fabrics: examples and applications from the McHugh Complex, Kenai Peninsula, Alaska. Journal of Structural Geology 21, 1773–1796.

Lister, G.S., Snoke, A.W., 1984. *S–C* mylonites. Journal of Structural Geology 6, 617–638.

Maltman, A.J., Byrne, T., Karig, D., Lallement, S., 1993. Deformation at the toe of an active accretionary prism: synopsis of results from ODP Leg 131, Nankai, SW Japan. Journal of Structural Geology 15, 949–964.

Moore, J.C., 1989. Tectonics and hydrogeology of accretionary prisms: role of the décollement zone. Journal of Structural Geology 11, 95–106.

Moore, J.C., 2000. Synthesis of results: logging while drilling, northern Barbados accretionary prism. In: Moore, J.C., Klaus, A. (Eds.). Proceedings of the Ocean Drilling Program Scientific Results, p. 171A.

Moore, J.C., Byrne, T., 1987. Thickening of fault zones: a mechanism of mélange formation in accreting sediments. Geology 15, 1040–1043.

Moore, J.C., Vrolijk, P., 1992. Fluids in accretionary prisms. Reviews of Geophysics 30, 113–135.

Moore, J.C., ODP Leg 171A Shipboard Scientific Party, 1998. Consolidation patterns during initiation and evolution of a plate-boundary décollement zone: northern Barbados accretionary prism. Geology 26, 811–814.

Onishi, C.T., Kimura, G., 1995. Change in fabric of melange in the Shimanto Belt, Japan: change in relative convergence? Tectonics 14, 1273–1289.

Osozawa, S., 1997. In situ basalts in Okinawa Island, and their tectonic significance. In: Miyashita, S. (Ed.). Significance of Greenstone for Accretionary Prism Development. Niigata University, Japan, pp. 1–5.

Taira, A., Ashi, J., 1993. Sedimentary facies evolution of the Nankai forearc and its implications for the growth of the Shimanto accretionary prism. Proceedings of the Ocean Drilling Program Scientific Results 131, 331–341.

Taira, A., Katto, J., Tashiro, M., Okamura, M., Kodama, K., 1988. The Shimanto Belt in Shikoku, Japan: evolution of Cretaceous to Miocene accretionary prism. Modern Geology 12, 5–46.

Ujiie, H., 1989. Eocene foreland thrust-fold belt of the central Ryukyu Island Arc: deduced from sedimentary structures in the Kayo Formation. In: Taira, A., Masuda, F. (Eds.). Sedimentary Facies in the Active Plate Margin. Terra Scientific Publishing Company, Tokyo, pp. 711–722.

Ujiie, H., 1994. Early Pleistocene birth of the Okinawa Trough and Ryukyu Island Arc at the northwestern margin of the Pacific: evidence from Late Cenozoic planktonic foraminiferal zonation. Palaeogeography Palaeoclimatology Palaeoecology 108, 457–474.

Ujiie, H., Nishimura, Y., 1992. Transect of the central and southern Ryukyu Island Arcs. 29th IGC Field Trip A24 Guidebook.

Ujiie, K., 1997. Off-scraping accretionary process under the subduction of young oceanic crust: the Shimanto Belt of Okinawa Island, Ryukyu Arc. Tectonics 16, 305–322.

Ujiie, K., Kinjo, M., Ujiie, H., 1997. Sedimentation and deformation process of the Eocene Kayo Formation in the Henoko area, the northern Okinawa Island. Bulletin of the College of Science University of the Ryukyus 64, 37–52.

Ujiie, K., Hisamitsu, T., Wonn, S., 2000. Magnetic and structural fabrics of the melange in the Shimanto accretionary complex, Okinawa Island: implication for strain history during decollement-related deformation. Journal of Geophysical Research 105, 25729–25741.